

Altered Growth and Branching Patterns in Synpolydactyly Caused by Mutations in HOXD13

Yasuteru Muragaki,* Stefan Mundlos,*† Joseph Upton, Bjorn R. Olsen

Hox genes regulate patterning during limb development. It is believed that they function in the determination of the timing and extent of local growth rates. Here, it is demonstrated that synpolydactyly, an inherited human abnormality of the hands and feet, is caused by expansions of a polyalanine stretch in the amino-terminal region of HOXD13. The homozygous phenotype includes the transformation of metacarpal and metatarsal bones to short carpal- and tarsal-like bones. The mutations identify the polyalanine stretch outside of the DNA binding domain of HOXD13 as a region necessary for proper protein function.

Vertebrates have four clusters of homeobox-containing genes (*HoxA*, *HoxB*, *HoxC*, and *HoxD*) that share a common ancestry with the *Drosophila Hom-C* complex. *Hox* genes are remarkably well conserved during evolution; the homeodomains not only have a high degree of amino acid identity, but they are also functionally conserved. Furthermore, both *Drosophila* and mammalian homeobox genes show the property of colinearity: Genes located more 3' within clusters are expressed earlier in development and more anteriorly than those located more toward the 5' end. The genes of the most 5' cluster, the *Abdominal-B* (*Abd-B*)-type *Hox* genes, have undergone a large expansion in number. Whereas there is a single gene in *Drosophila*, there are a total of 15 *Abd-B*-type genes in vertebrates (1).

Studies of developing limbs suggest that this group of genes is involved in limb development (2–5), but the molecular mechanisms by which they act are not known. *Hox* genes are composed of at least two regions: a 3' region of 180 base pairs (bp) (the homeobox) encoding a DNA binding motif (the homeodomain) and a large 5' region encoding sequences that could be involved in interactions with other proteins. Although the function of the homeodomain has been studied in detail (6, 7), less is known about the function or functions of the NH₂-terminal region of *Hox* proteins. Here we report that a limb abnormality in humans, synpolydactyly, is caused by in-frame insertions in the NH₂-terminal, non-DNA binding part of HOXD13 protein. Alterations in the carpal-metacarpal and tarsal-metatarsal regions indicate that the insertions

define a functionally important domain of HOXD13.

Syndactyly and polydactyly are common malformations that present, respectively, as webbing between fingers and duplication of fingers. Type II syndactyly or synpolydactyly (SPD) (OMIM number 186000) is one example of a genetically determined isolat-

ed limb abnormality involving both webbing and duplications. SPD is generally considered to be an autosomal, dominantly inherited trait with incomplete penetrance (estimated to be 96%) (8). Three families investigated in this study (pedigrees I, II, and III) have the typical features previously described (8) for SPD consisting of variable syndactyly of digits III and IV with an additional digit in between (Fig. 1A). In most cases the extra digit arose through the formation of an additional metacarpal between metacarpals III and IV with more or less normal distal phalanges (Fig. 1B). The supernumerary metacarpal was found either separate or fused to either of the neighboring metacarpals. In some instances the metacarpals were normal but the phalanges of digit III or IV were duplicated. In the feet, syndactyly of toes III, IV, and V was observed, usually together with postaxial polydactyly (9).

One individual, II-8 (from pedigree II), had a different phenotype, which first suggested a different diagnosis (Fig. 1, C and

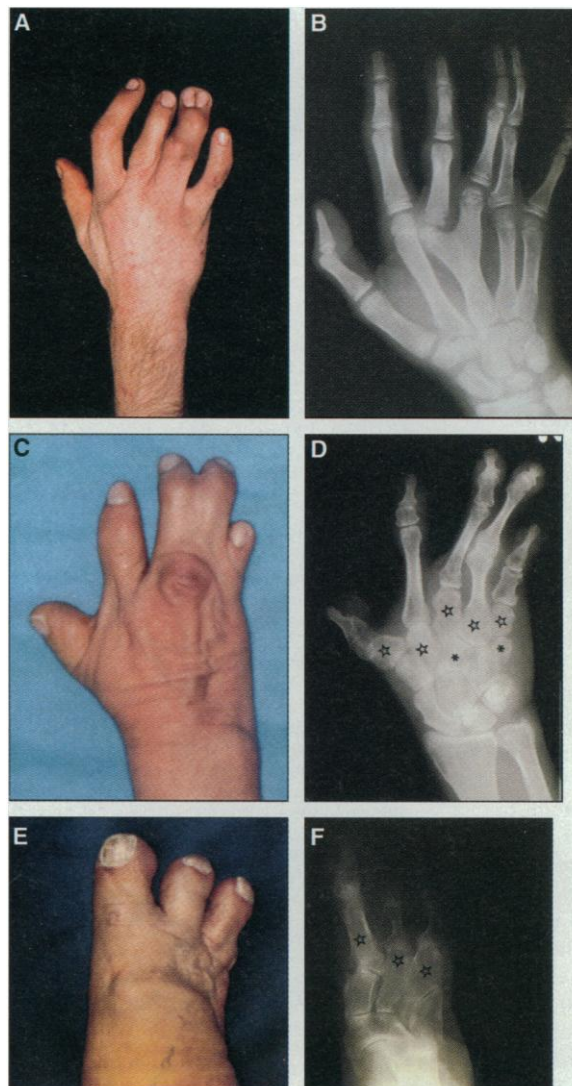


Fig. 1. Photographs and x-rays showing the synpolydactyly phenotype. Hand (A) and x-ray (B) of a heterozygous individual indicated by arrow in pedigree II in Fig. 3. Note the branching of metacarpal III and the resulting extra digit IIIa. The syndactyly between digits has been partially corrected by surgical separation of III and IIIa-IV. (C) and (D) show hand and x-ray of homozygous individual II-8 of pedigree II (Fig. 3). Note syndactyly of digits III, IV, and V, their single knuckle, the transformation of metacarpals I, II, III, and V to short carpal-like bones (stars), two additional carpal bones (asterisks), and short second phalanges. The radius, ulna, and proximal carpal bones appear normal. (E) and (F) show foot and x-ray of homozygous individual II-8 of pedigree II. Note the relatively normal size of metatarsal I, the small size of metatarsal II, and the replacement of metatarsal III, IV, and V with a single tarsal-like bone (stars).

Y. Muragaki, S. Mundlos, B. R. Olsen, Department of Cell Biology, Harvard Medical School, Boston, MA 02115, USA.

J. Upton, Department of Surgery, Division of Plastic Surgery, Beth Israel and Children's Hospital, Harvard Medical School, Boston, MA 02115, USA.

*These authors are joint first authors.

†To whom correspondence should be addressed.

D). However, analysis of her pedigree (see below) revealed that her parents were first cousins, with her mother having an SPD-like phenotype, and she had two affected sons of which one (Fig. 1, A and B) was available for phenotypic analysis. Clinical and x-ray evaluation demonstrated classical SPD (Fig. 1, C and D). Thus, individual II-8 was considered most likely homozygous for the SPD mutation with one of her parents being a nonpenetrant carrier. Her hands (Fig. 1, C and D) and feet (Fig. 1, E and F) were very small. All of her digits were very short, and there was syndactyly between digits III, IV, and V in the hands; her feet had only three digits. X-rays showed a normal radius and ulna and nor-

mal proximal carpals. The metacarpals were extremely short and had, with the exception of metacarpal IV, the appearance of carpal bones. The trapezoid could not be distinguished, and two accessory bones were present next to the capitate and the hamate (Fig. 1D). In addition, phalanx 2 of digit I was duplicated, and phalange 2 of digits II through V was very short. In the feet, metatarsal II was very short and metatarsals III, IV, and V were replaced by one short tarsal-like bone.

With the use of a candidate gene approach we genetically mapped SPD to chromosome 2q. This region of the human genome contains the *HOXD* cluster and several other genes that are related to limb

development and was thus considered a good candidate region. Linkage was established along a 2-centimorgan interval between markers D2S111 and D2S1391. This interval was accurately positioned by the use of an intragenic dinucleotide repeat polymorphism that is located within the *HOXD8* gene (10). These results closely linked SPD to the *HOXD* cluster. Similar linkage data have been demonstrated by other investigators (11, 12). The *HOXD* cluster on chromosome 2q31-32 contains nine homeobox genes (*HOXD1*, *-D3*, *-D4*, *-D8*, *-D9*, *-D10*, *-D11*, *-D12*, and *-D13*); *EVX2*, a homeobox gene related to the *Drosophila even-skipped* gene; and two homeobox genes related to the *Drosophila distal-less* gene (*DLX1* and *DLX2*) (13). *HOXD9* through *HOXD13* and *EVX2*, *DLX1*, and *DLX2* are expressed in the developing limb bud. Of these candidate genes *HOXD12*, *HOXD13*, and *EVX2* were analyzed because these genes are expressed in the most distal part of the limb bud, the autopod (14, 15). Sequencing of the homeoboxes of all three genes revealed no base change. With a cosmid that contains *EVX2* and *HOXD10* through *HOXD13* (13), we cloned the human 5' sequence (exon 1) of *HOXD12* and *HOXD13* (16). The sequence of *HOXD13* revealed that the protein contained two serine stretches and one alanine stretch consisting of 15 amino acid residues (Fig. 2A). Amplification of the sequence coding for the alanine stretch showed an additional larger band in all affected individuals of all three pedigrees (Fig. 3) (17). Sequencing of the wild-type and the enlarged amplification product demonstrated 21-bp, 24-bp, and 30-bp duplications, all within the alanine coding region, in pedigrees II, I, and III, respectively (Fig. 2, B and C). Polymerase chain reaction (PCR) amplification and sequencing of DNA from individual II-8 confirmed the initial clinical presumption that this patient is homozygous for the mutation (Fig. 3). Individual III-14, who was clinically unaffected, is heterozygous for the mutation and is thus a nonpenetrant carrier. PCR analysis of DNA from 56 unrelated normal control individuals showed only the presence of the wild-type product. This, combined with the fact that pedigree I represents a sporadic, nonfamilial case of SPD, makes a compelling argument that the mutations are indeed causative for the phenotype.

Polyalanine tracts, similar to that found in the *HOXD13* amino acid sequence, have been observed in other transcription factors such as the *Drosophila* proteins even-skipped, engrailed, or Krüppel (18-20). These proteins act as transcriptional repressors, with the alanine-rich regions being (in addition to the homeodomain) essential for strong repression (21, 22). The expansion

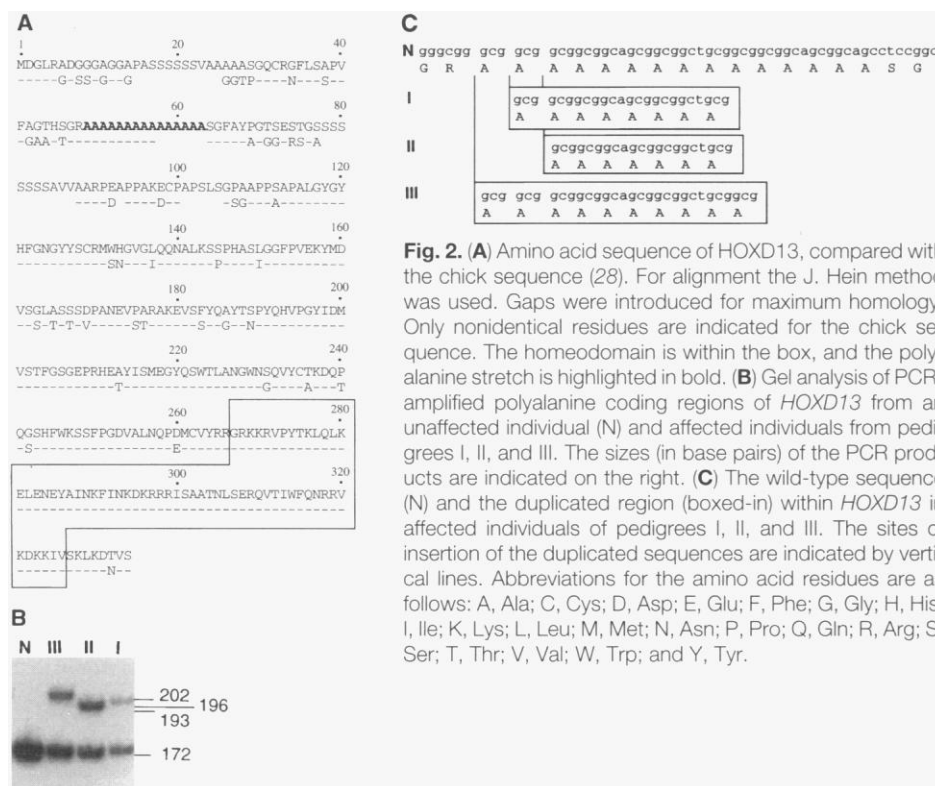
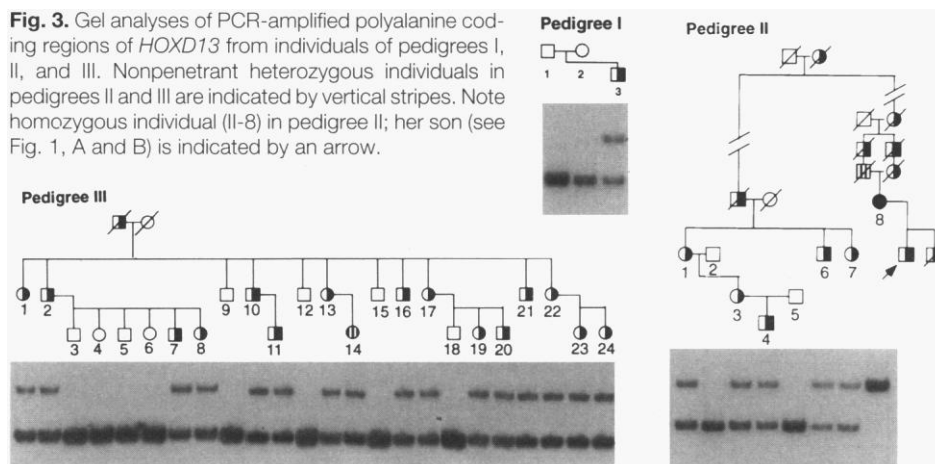


Fig. 2. (A) Amino acid sequence of *HOXD13*, compared with the chick sequence (28). For alignment the J. Hein method was used. Gaps were introduced for maximum homology. Only nonidentical residues are indicated for the chick sequence. The homeodomain is within the box, and the polyalanine stretch is highlighted in bold. (B) Gel analysis of PCR-amplified polyalanine coding regions of *HOXD13* from an unaffected individual (N) and affected individuals from pedigrees I, II, and III. The sizes (in base pairs) of the PCR products are indicated on the right. (C) The wild-type sequence (N) and the duplicated region (boxed-in) within *HOXD13* in affected individuals of pedigrees I, II, and III. The sites of insertion of the duplicated sequences are indicated by vertical lines. Abbreviations for the amino acid residues are as follows: A, Ala; C, Cys; D, Asp; E, Glu; F, Phe; G, Gly; H, His; I, Ile; K, Lys; L, Leu; M, Met; N, Asn; P, Pro; Q, Gln; R, Arg; S, Ser; T, Thr; V, Val; W, Trp; and Y, Tyr.



of the alanine tract as observed in our SPD patients may thus alter the function of HOXD13. This alteration is unlikely to be a straightforward loss of function, because mice with a targeted disruption of *Hoxd13* do not show an SPD-like phenotype (23). There are similarities, such as shortening and thickening of the metacarpals, shortening of the second phalanges, and the appearance of an extra digit, but the overall phenotype is clearly different from and weaker than that of the affected individuals described here. One possibility is that complete disruption of *Hoxd13* may not lead to a dramatic phenotype because its function may be partially compensated for by *Hoxd11* and *Hoxd12*. In contrast, the mutant SPD protein may still be able to participate in DNA binding but may not, through its mutated NH₂-terminal region, be able to engage in productive protein-protein interactions.

Another possibility is that the mutation affects the cooperative interaction of HOXD13 with other *Hox* genes and transcription factors. During mouse limb development the *Abd-B* subfamily of the *HoxA* cluster (*Hoxa10*, *Hoxa11*, and *Hoxa13*) are expressed in restricted domains along the proximal-distal axis of the limb bud with *Hoxa10* being mainly expressed in the upper limb (stylopod), *Hoxa11* in the lower limb (zeugopod), and *Hoxa13* in the hand and foot (autopod) (24). Genes of the *Abd-B HoxD* complex (*Hoxd11* through *Hoxd13*) are expressed initially along the anteroposterior axis in a nested set centered around the zone of polarizing activity (14). As the autopod develops, the pattern shifts from anterior-posterior to proximal-distal so that their expression covers the entire autopod. Within the *HoxD* complex *Hoxd13* has the most anterior border of expression including digit I (25). In the late phase of *Hox* gene expression, the proximal boundary of *Hoxa13* is located more proximal than the proximal boundary of *Hoxd13*, leaving a re-

gion of nonoverlap that is located in the future wrist region (23–25). If *Hoxa13* determines round, carpal bone morphology, as suggested by overexpression experiments (5), it is likely that the interaction with *Hoxd13* produces the long bones of the digits. In humans, an alteration in HOXD13 that affects its interaction with HOXA13, for example, could conceivably lead to changes in growth rates and sizes of the cartilage anlagen in the most proximal part of the HOXD13 region of expression, thus explaining why the metacarpals and metatarsals are short, carpal- and tarsal-like bones in the homozygote (Fig. 1, C, D, E, and F).

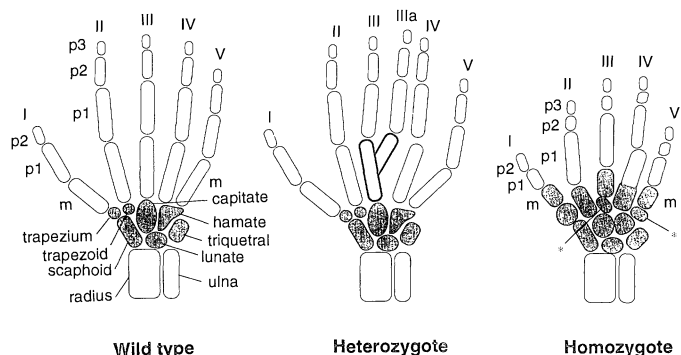
The development of the tetrapod limb can be interpreted as a series of condensation, branching, and segmentation events. Shubin and Alberch (26) proposed a model in which the autopod represents a skewing of the primary axis of the limb in that the main axis of condensations (the metapterygial axis) runs from the ulna through the ulnare (triquetrum) and then bends anteriorly through the distal carpals (the digital arch). In primitive fish the expression of *Hoxd11* does not bend anteriorly, as observed in tetrapods, but maintains a posterior restriction (27). The fish fin thus appears like a truncated limb without autopod. It seems somewhat paradoxical that teleost fish and mammals, albeit their vastly different phenotypes, have the same number of *Hox* clusters that contain the same set of genes. Evolutionary new structures such as the autopod would thus require the acquisition of new functions for *Hox* genes. Such a functional expansion could be accomplished by a change in the timing, the position, or level of *Hox* gene expression, or changes in the regulatory interactions between *Hox* proteins and their targets. In this respect it is of interest that the mutations described here disrupt a domain of *Hoxd13* that is evolutionarily not conserved. The alanine stretch observed in the human HOXD13 sequence is absent in

the zebrafish (*Danio rerio*) (27). In contrast, the chick 5' HOXD13 sequence encodes 9 alanine residues as compared with 15 residues encoded by the human sequence (28). Thus, during the evolution from fish to tetrapods an alanine stretch was introduced, and then during the evolution of mammals the residues were almost doubled. It is thus possible that alterations in the NH₂-terminal region of the *Hoxd13* sequence (and that of other *Hox* genes) play a role in the acquisition of new functions. In tetrapods such a new function of *Hoxd13* may be to determine local growth rates within the developing digital arch. The mutations described here may cause alterations in these processes so that some of the digital anlagen form improperly (heterozygous individuals) or are converted into short carpal-like bones (homozygous individual) (Fig. 4). Overexpression of the human wild-type and mutant HOXD13 sequences with alanine runs of different lengths through the use of retroviral vectors in chick embryos should allow a testing of this possibility.

REFERENCES AND NOTES

1. S. B. Carroll, *Nature* **376**, 479 (1995).
2. B. A. Morgan and C. Tabin, *Dev. Suppl.* **1994**, 181 (1994).
3. D. J. Roberts and C. Tabin, *Am. J. Hum. Genet.* **55**, 1 (1994).
4. B. A. Morgan, J. C. Izpisua-Belmonte, D. Duboule, C. J. Tabin, *Nature* **358**, 236 (1992).
5. Y. Yokouchi *et al.*, *Genes Dev.* **9**, 2509 (1995).
6. W. J. Gehring *et al.*, *Cell* **78**, 211 (1994).
7. D. L. Smith and A. D. Johnson, *EMBO J.* **13**, 2378 (1994).
8. B. S. Sayli *et al.*, *J. Med. Genet.* **32**, 421 (1994).
9. Y. Muragaki, S. Mundlos, J. Upton, B. R. Olsen, unpublished observations.
10. D. R. Rosen and R. H. Brown Jr., *Hum. Mol. Genet.* **2**, 617 (1993).
11. M. Sarfarazi, A. N. Akarsu, B. S. Sayli, *ibid.* **4**, 1453 (1995).
12. M. H. Polymeropoulos, R. I. Ortiz deLuna, S. E. Ide, C. A. Francomano, *Am. J. Hum. Gen.* **57** (suppl.), A200 (1995).
13. M. D'Esposito *et al.*, *Genomics* **10**, 43 (1991).
14. J. C. Izpisua-Belmonte, C. Tickle, P. Dollé, L. Wolpert, D. Duboule, *Nature* **350**, 585 (1991).
15. P. Dollé, V. Fraulob, D. Duboule, *Dev. Suppl.* **1994**, 143 (1994).
16. For sequencing of exon 1 of the HOXD13 gene the cosmid clone G2 (15), containing the homeobox genes HOXD10, HOXD11, HOXD12, HOXD13, and EVX2, was digested with Eco RI, and a 10-kb fragment containing the entire HOXD13 and the 5' half of the HOXD12 gene was subcloned in the Eco RI site of pBluescript. With this fragment as a template, the sense primer 5'-TTTGTATCAGGGGATGTGGC-3' and the antisense primer 5'-CCATACAGGAGACAGTATC-3' were used to amplify exon 2 of the HOXD13 gene by PCR. A 1.3-kb Pst I fragment derived from the 10-kb Eco RI fragment hybridized with the PCR product and was therefore subcloned in the Pst I site of pBluescript and sequenced by dideoxynucleotide cycle sequencing. Because the 5' end of the sequence of the Pst I fragment did not reach the translational start codon ATG of the HOXD13 gene, the primer 5'-ACATACGGCAGCTGTAGTAG-3', corresponding to a sequence 70 bp downstream of the 5' Pst I site, was used for sequencing with the 10-kb Eco RI fragment as the template.
17. For analysis of the HOXD13 gene in affected and nonaffected individuals, genomic DNA was extract-

Fig. 4. Diagrams of the hand skeleton of heterozygous and homozygous individuals with synpolydactyly (see Fig. 1) compared with a normal (wild-type) hand. Carpal bones are shaded. The pisiform bone is not shown. Digits are indicated by Roman numerals, metacarpals are indicated by the letter m, and the phalanges are indicated by p1, p2, and p3. In the heterozygote, metacarpal III is branched and gives rise to an extra digit IIIa. In the homozygote, the metacarpals are fully (metacarpals I, II, III, V) or partially (metacarpal IV) replaced by carpal-like bones. Two additional carpal bones are indicated by asterisks. The trapezoid is absent. Note also the short p2 in all digits.



ed from whole blood by Puregene (Gentra System). The sense primer 5'-CAGRCCGCGGCTTCT-TCTC-3' and the antisense primer 5'-CTACAACG-GCAGAAGAGGAC-3' were designed to amplify the 172-bp NH₂-terminal region of HOXD13 containing the 15 alanine residues. PCR was performed with [α -³²P]deoxycytidine 5'-triphosphate (dCTP) (10 mM, 3000 Ci/mmol) added to the reaction. The condition was 35 cycles at 94°C for 0.5 min, 60°C for 1 min, 72°C for 2 min, with initial heating at 95°C for 2 min and, after all 35 cycles were completed, additional heating at 72°C for 10 min. PCR reactions were performed in a total volume of 10 μ l containing 1 \times PCR buffer, 0.75 mM MgCl₂, 200 μ M deoxynucleotide triphosphate (dNTP) without dGTP, 200 μ M 7-deaza-2'-deoxyguanosine 5'-triphosphate, a final concentration of 0.5 μ M for each prim-

er, 10% dimethyl sulfoxide, and 0.2 U of Taq polymerase. The PCR products were analyzed on a 5% polyacrylamide gel under non-denaturing conditions. PCR products from affected individuals were subcloned into pCR11 (Invitrogen) and subjected to cycle sequencing.

18. S. Hayashi and M. P. Scott, *Cell* **63**, 883 (1990).
 19. J. B. Jaynes and P. H. O'Farrell, *Nature* **336**, 744 (1988).
 20. J. D. Licht, M. J. Grossel, J. Figge, U. M. Hansen, *ibid.* **346**, 76 (1990).
 21. K. Han and J. L. Manley, *Genes Dev.* **7**, 491 (1993).
 22. ———, *EMBO J.* **12**, 2723 (1993).
 23. P. Dolle *et al.*, *Cell* **75**, 431 (1993).
 24. Y. Yokouchi, H. Sasaki, A. Kuroiwa, *Nature* **353**, 443 (1991).

25. P. Dolle, J. C. Izpisua-Belmonte, E. Boncinelli, D. Duboule, *Mech. Dev.* **36**, 3 (1991).
 26. N. H. Shubin and P. Alberch, *Evol. Biol.* **20**, 319 (1986).
 27. P. Sordino, F. van der Hoeven, D. Duboule, *Nature* **375**, 678 (1995).
 28. B. Rogina and W. B. Upholt, *Nucleic Acids Res.* **21**, 1316 (1993).
 29. The cosmid clone G2, containing the HOXD13 gene, was provided by E. Boncinelli. We want to thank C. Tabin for helpful discussions. Y. Pittel provided secretarial assistance. Supported by NIH grants AR36819 and AR36820 (to B.R.O.) and Deutsche Forschungsgemeinschaft (to S.M.).

18 January 1996; accepted 13 March 1996

Interactions Between Electrical Activity and Cortical Microcirculation Revealed by Imaging Spectroscopy: Implications for Functional Brain Mapping

Dov Malonek and Amiram Grinvald

Modern neuroimaging techniques use signals originating from microcirculation to map brain function. In this study, activity-dependent changes in oxyhemoglobin, deoxyhemoglobin, and light scattering were characterized by an imaging spectroscopy approach that offers high spatial, temporal, and spectral resolution. Sensory stimulation of cortical columns initiates tissue hypoxia and vascular responses that occur within the first 3 seconds and are highly localized to individual cortical columns. However, the later phase of the vascular response is less localized, spreading over distances of 3 to 5 millimeters.

Regional changes in cerebral blood flow and blood oxygenation "co-localize" with regions of increased neuronal activity (1, 2). Signals that reflect these changes have been used by positron-emission tomography (PET) and functional magnetic resonance imaging (f-MRI) to both understand cortical metabolism and investigate cognitive and perceptual processes by rapid identification of functionally distinct cortical areas (3, 4). Furthermore, the study of spatial relationships between individual cortical columns within a given brain area has become feasible with optical imaging based on intrinsic signals, at a spatial resolution of about 50 μ m (5–7). However, there are outstanding controversies concerning whether cortical metabolism is aerobic or anaerobic, and indeed, the physiological events underlying these secondary signals have not been fully assessed (2, 3). It is necessary to clarify the spatiotemporal characteristics of the intrinsic signals (8) in order to reveal the electrical activity underlying these signals and assess cognitive functions. Such clarification would set fundamental limits on the spatial and temporal resolutions for several functional brain imaging techniques.

Here we characterize the spatial preci-

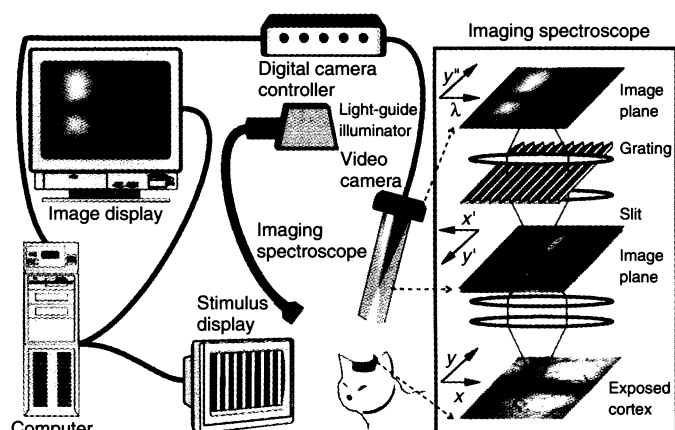
sion and dynamics of blood oxygenation signals using in vivo intrinsic optical signals reflected from the exposed visual cortex. Previous optical imaging studies (5, 9) suggested that the intrinsic signal observed in vivo is composed of several components, each of which reflects different vascular and metabolic sources. However, the temporal dynamics and spatial precision of these components were not determined.

To identify the spatiotemporal charac-

teristics of the individual components of the intrinsic signal at many cortical locations, we designed the imaging spectroscopy illustrated schematically in Fig. 1. A narrow, slitlike region from the exposed cortex of an anesthetized cat was projected onto a dispersing grating and focused on the camera detector. The image thus obtained represents multiple displaced versions of the isolated "slitlike cortical image," each of which is displaced as a function of wavelength. From the intensity variations in this spatio-spectral image (y'' , λ), we obtained the reflection spectrum of each imaged cortical point. In other words, the intensity profile of each horizontal line represented the reflection spectrum of a given location in the imaged cortex. The intensity profile along a vertical line represented the spatial pattern of cortical activation at a given wavelength. During the experiment, a sequence of such spatio-spectral images was recorded after sensory stimulation.

Several important features of the spatio-spectral image are immediately apparent in Fig. 2. Large absorption (lower intensity of reflection, dark image) is evident at the wavelength range of 500 to 600 nm, and significantly less light was absorbed (higher intensi-

Fig. 1. The system for standard optical imaging (6, 11, 22). The inset at the right shows the scheme of the imaging spectroscopy. It contains two tandem-lens macroscopes, diffraction grating (22), and an opaque disk with a transparent slit. The cortical surface (bottom image) is illuminated with white light ($\lambda = 500$ to 700 nm) and imaged through the first macroscope onto the first image plane, where an opaque disk with a slit is positioned. The light thus isolated is collimated, passed through a diffraction grating whose light dispersion is perpendicular to the slit, and then focused on the camera target (top image). The axes show the different optical transformations that the cortical image undergoes. Temporal resolution was up to 100 ms. Spectral resolution, 1 to 4 nm.



Department of Neurobiology, Weizmann Institute of Science, Rehovot 76100, Israel.